International Journal of Mass Spectrometry 298 (2010) 91–98

Contents lists available at ScienceDirect

International Journal of Mass Spectrometry

journal homepage: www.elsevier.com/locate/ijms

Residual counter ions can stabilise a large protein complex in the gas phase☆

Joanna Freeke, Carol V. Robinson**, Brandon T. Ruotolo*

University of Cambridge, Department of Chemistry, Lensfield Road, Cambridge CB2 1EW, United Kingdom

ARTICLE INFO

Article history:
Received 18 December 2008
Received in revised form 21 July 2009
Accepted 3 August 2009
Available online 12 August 2009

Keywords:
Nano-electrospray ionisation (nano-ESI)
Non-covalent complexes
Accurate mass determination
Collision-induced dissociation (CID)
Ion mobility–mass spectrometry (IM–MS)

ABSTRACT

The dual goals of retaining native solution structure in the gas phase and facilitating accurate mass measurement by mass spectrometry often require conflicting experimental parameters. Here, we use ion mobility–mass spectrometry to investigate the effects of aqueous buffer removal on the structure of an archetypal ring complex, GroEL, an 800 kDa chaperone protein complex from *Escherichia coli*. Our data show that subjecting the protein complex ions to energetic collisions in the gas phase removes aqueous buffer from the assembly in a manner indicative of at least two populations of adducts bound to the complex. Adding further energy to the system disrupts the quaternary structure of the assembly, causes monomer unfolding, and eventual dissociation at higher collision energies. Including additional salts of lower volatility in a typical ammonium acetate buffer produces gas-phase protein complex ions that are seemingly stabilised relative to changes in gas-phase structure. These data are combined to offer a general picture of the desolvation and structural transitions undergone by large gas-phase protein complexes.

1. Introduction

Mass spectrometry (MS) is becoming established as a key technology in structural biology, yielding data on protein dynamics, ligand binding and protein complex structure [1–6]. For example, recent work has shown that MS data, composed of mass measurements taken at every level of protein organisation (intact, sub-complexes, and subunits), can generate high confidence interaction maps and, in some cases, 3-D models of protein assemblies can be constructed [7–10]. Such assemblies, often comprising a large number of subunits, can result in protein complexes with masses in excess of 1 MDa—challenging targets for accurate MS measurements. However, careful optimisation of instrument conditions has been shown to facilitate both a mass range sufficient to study systems as large as the ribosome [11] and virus assemblies [12] as well as mass resolution that is adequate for following the subunit exchange dynamics within many protein assemblies [13,14].

The analysis of intact protein–protein complexes relies upon ionisation methods that can retain non-covalent protein–protein interactions, such as nano-electrospray ionisation [15,16] (nESI). From a solution of only a few microlitres in volume, nESI produces a fine mist of charged droplets which decrease rapidly in size by evaporation. As these droplets shrink, their size/charge ratio approaches the Raleigh limit, resulting in a series of coulombically driven fission events that produce a large number of daughter droplets from a single parent. For large analytes, such as protein complexes, this fission process is believed to continue until the droplets are small enough (droplet diameter ≈ 20 nm) such that the excess aqueous buffer surrounding the protein complex evaporates to produce a gas-phase ion (termed the charge residue model (CRM)) [17,18]. Recent analysis of protein and protein complex data indicate that the amount of charge accumulated by large ions correlates well with estimates of ion surface area [18–20]. The dependence is predicted by the CRM and these results are consistent with this model for describing the primary mode in which protein assembly ions are generated.

Due to incomplete evaporation in the nESI process, or the presence of species of low volatility in solution, the protein complex ions detected by MS usually contain some residual molecules derived from aqueous buffer [21,22]. Their presence reduces both the mass accuracy and the peak resolution, and therefore the quality of spectral information obtained. A linear relationship between peak width and mass increase has been derived empirically over a broad range of proteins and instrument conditions [23]. While this approach can produce accurate mass measurements for large protein complexes, achieving the necessary accuracy for unambiguous assignment is still a challenge. Consequently mass measurements of protein assemblies are usually performed using the largest accel-

Abbreviations: MS, mass spectrometry; IM, ion mobility; nESi, nano-electrospray ionisation; ESI, electrospray ionisation; CRM, charge residue model; CID, collision-induced dissociation; %CCS, percentage collision cross-section; LRWH, linearly ramped wave height; PA, projection approximation; EHSS, exact hard spheres scattering; Q-ToF, quadrupole time of flight.

☆ This article is part of a Special Issue on Ion Mobility.

* Corresponding author. Department of Chemistry, University of Michigan, 930 N University Ave, Ann Arbor MI 48109, United States. Tel.: +44 1223 763844; fax: +44 1223 763843.

** Corresponding author. Tel.: +44 1223 763846; fax: +44 1223 763843.

E-mail addresses: cvr24@cam.ac.uk (C.V. Robinson), bruotolo@umich.edu (B.T. Ruotolo).

1387-3806/$ – see front matter © 2009 Elsevier B.V. All rights reserved.
doi:10.1016/j.ijms.2009.08.001

eration voltages accessible that maintain the subunit interactions of the complex [24,9].

Conversely, nESI is able to preserve aspects of native protein structure when only the lowest acceleration voltages are applied, as shown by collision cross-section (CCS) measurements derived from ion mobility (IM) separation [6,25–27]. IM records the time an ion takes to pass through a pressurised drift cell in the presence of a weak applied electric field [28–32]. Large ions of low charge yield longer drift times than more compact architectures or those that have higher charge. For experiments involving protein–protein complexes, and indeed many other IM experiments aimed at structural biology, a crucial consideration is the ability to maintain solution phase topology in the absence of bulk solution. Previous experiments from our group and others have indicated that, if instrument conditions are not carefully controlled, protein assemblies can adopt a wide array of conformations, some of which appear to be stable on the timescale of the IM experiment [33,34]. While nESI can generate protein complex ions for analysis by both IM and MS, the instrument conditions required for optimum analysis for each of these two dimensions of information do not fully overlap [33]. It is reasonable to assume that the solution phase topology is best preserved by maintaining as much aqueous buffer as possible. Previous data indicate that minimising the internal energy of the protein complex ions is also important for retaining "native-like" structure in the gas phase. On the other hand, the greatest mass accuracy, by definition, requires the most efficient removal of buffer ions [24]. As such, accurate mass measurements of large protein complexes in general require maximum acceleration voltages, generating high internal energies, and, as a consequence, altered protein structures.

Here, we use ion mobility mass spectrometry (IM–MS) to investigate how the structure and mass of a protein complex ion are influenced by changes in aqueous buffer composition. This is studied by varying the energy applied to the ions (and therefore varying the number of residual buffer ions/molecules attached to the assembly) and recording the effect on both assembly size and mass by IM–MS. We have chosen to study the bacterial chaperone GroEL (comprising 14 identical subunits arranged in two back-to-back rings), as it is a well-studied protein complex by mass spectrometry and structural biology [5,35,36]. The presence of a cavity within the quaternary structure of GroEL opens the possibility of observing structural transitions in the gas-phase complex by IM–MS, in a similar way to those reported previously [25]. Furthermore, this allows the impact of different buffer components on the stability of the quaternary structure of GroEL in the gas phase to be compared and provides a framework for recording the measurable desolvation and structural transitions in the electrospray process for a large protein complex.

2. Materials and methods

2.1. Sample preparation

Freeze-dried GroEL (C7688) was purchased from Sigma–Aldrich (Dorset, UK) and 1 mg was dissolved and incubated (1 h) in 160 μl buffer A (20 mM tris acetate, 50 mM EDTA, 1 mM ATP, 5 mM magnesium chloride), after which 40 μl methanol was added and incubated (1 h). GroEL was precipitated by adding 200 μl acetone and the precipitate re-suspended in 200 μl buffer A before size exclusion chromatography in 200 mM ammonium acetate (Sigma–Aldrich). In some cases this chromatography step was repeated for sufficient purity. The fractions collected were concentrated to a final GroEL concentration of approximately 2 μM 14mer on a Vivaspin column (MWCO 5000, Sartorius, Epsom, UK). Tris acetate (Sigma–Aldrich) was dissolved in 200 mM ammonium acetate and added into some of the solutions for analysis (final concentrations of 25 and 50 mM tris acetate in 200 mM ammonium acetate and pH of 6.9).

2.2. Mass spectrometry

MS analysis was carried out on a modified Q-ToF II [37] and a Synapt HDMS quadrupole–ion trap–IM–MS instrument [38] (Waters, Manchester, UK). Nanoflow electrospray capillaries were prepared as previously described [25], and a nESI source was used. MS parameters were optimised for the transmission of large non-covalent complexes. Typical values are: capillary voltage 1.2 kV, cone voltage 150 V, cone gas 80 litres h^{-1}, extractor 0.3 V, ion transfer stage pressure 5.00 mbar, transfer voltage 12 V, bias 70 V, varied trap voltage 5–240 V, IMS wave velocity 250 m/s, IMS wave height either ramped or varied between 10 and 16 V, transfer wave velocity 100 m/s, transfer wave height 5 V, trap and transfer pressure 5.48×10^{-2} mbar, IMS pressure 5.08×10^{-1} mbar, ToF analyser pressure 1.85×10^{-6} mbar.

Large non-covalent complexes such as GroEL require the application of acceleration voltage and energetic collisions for optimum mass accuracy. For Q-ToF mass spectrometers, ions are often accelerated into a gas-filled collision cell region just after the quadrupole mass filter. In the case of the Q-IM-ToF mass spectrometer (Synapt), ion acceleration and activation can be performed in many regions of the instrument. For all of the data reported in this work the amount of acceleration voltage experienced by the ions was varied as they enter the ion trap, just prior to the IM separation stage.

Spectra were analysed using MassLynx V4.1. The primary sequence mass from the UniProt database (http://www.uniprot.org/uniprot/P0A6F5), after removal of the N-terminal methionine from the unmodified precursor sequence, gives rise to a mass of 57197.9 Da for the monomer (confirmed by MS) and 800770.6 Da for the 14mer. Percentage mass increase and normalised peak width are calculated using the equations below.

$$\textit{Percentage Mass Increase} = \left[\frac{\textit{Centroid Experimental Mass}}{\textit{Sequence Mass}}\right] \times 100$$

$$\textit{Normalised Peak Width} = \frac{\textit{Full Width at Half Maximum}}{\textit{Centroid } m/z \textit{ Value}} = \frac{1}{\textit{Resolving Power}}$$

The centre-of-mass energy (E_{CoM}) was calculated from the formula derived by Shukla [39] $E_{CoM} = m_1/(m_1 + m_2) \times z\ V$, where m_1 is the mass of the collision gas molecules (argon), m_2 is the mass of the analyte ions (GroEL), z is the charge on the analyte and V is the acceleration voltage applied to the analyte as it enters the collision cell of the Q-ToF II mass spectrometer or the trap region of the Synapt HDMS. The upper bound collision energy required to remove a tris ion from the complex was estimated from the data in Fig. 4. The calculation consisted in plotting the initial desolvation gradients against tris concentration, and from a linear fit to this data the energy to remove an ion of 122 Da mass (tris) was averaged for this range of concentrations.

The percentage collision cross-section (%CCS) increase was taken from data acquired on the Synapt using both fixed and linearly ramped wave height (LRWH, wave height ramp from 0 to 30 V) over the course of the ion mobility separation. The CCSs acquired from fixed wave height data were calibrated externally as described previously [32]. Due to the projected size of GroEL (computational estimate of the CCS of GroEL from the crystal structure is ca. 21,000 $Å^2$ [40,41], see below for details) we used a calibration dataset including ions of significantly larger sizes and lower mobilities than used previously. These ions were the 5mer and 10mer

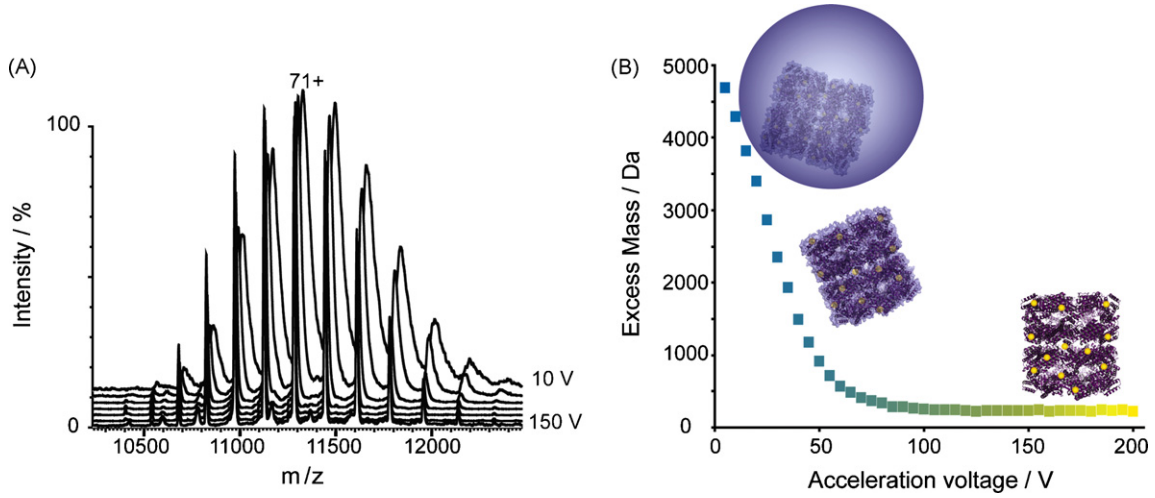

Fig. 1. Panel A shows the spectra of GroEL over a range of acceleration voltages applied to the ions to produce energetic collision with neutral gas molecules. The back spectrum is taken at 10 V acceleration voltage and spectra recorded at higher acceleration voltages are overlaid. Panel B contains a plot of the measured excess mass relative to the sequence mass of GroEL versus the acceleration voltage. Points are colour coded to indicate the internal energy of the ions, with blue indicating low and yellow indicating high internal energy. Overlaying the data is a schematic of GroEL in a droplet, with a rough "solvation shell" and with only tightly bound adducts remaining. Light purple regions depict the "solvation shell" comprising weakly bound water and aqueous buffer, while yellow circles represent tightly bound adducts. (For interpretation of the references to colour in this figure legend, the reader is referred to the web version of the article.)

of serum amyloid protein (average measured CCSs of 5876 and 8888 Å^2 respectively) as well as the 64–67$^+$ ions of GroEL (average measured CCS of 17415 Å^2). The absolute CCS for these ions (to an approximate error of ±5% based on a limited comparison with literature values) was determined using a recently reported method, that records the wave height necessary for an ion to transition between "ion mobility separation mode" and transmission mode (which carries all ions at the wave velocity), on the Synapt HDMS instrument [42]. We also used this direct measurement technique [42] to measure the size increase at high acceleration voltage and generated values comparable to those reported in Fig. 4. Data acquired in a LRWH mode often produce more well-resolved IM–MS data than when operated at fixed wave height, but are more difficult to calibrate to a CCS axis due to the constantly scaling drift force applied to the ions. In all cases where LRWH data were collected to assess the relative size of GroEL ions, equivalent data were acquired at several fixed wave heights for the purposes of calibration.

MOBCAL [40,41] (http://www.indiana.edu/~nano/Software.html) simulations of GroEL crystal structure (PDB code 1SX3) were carried out to determine computational CCS using the projection approximation (PA) and exact hard spheres scattering (EHSS) methods. This PDB file was also manipulated using Pymol (DeLano Scientific, http://pymol.org/) to prepare a fully extended GroEL subunit (setting all Φ and Ψ angles to 180°), which was docked onto the structure of 13 GroEL subunits using Hex 5.0 [43] (http://www.csd.abdn.ac.uk/hex/). This docked file of the 14mer containing one fully extended subunit was used to generate a computational CCS value for this structure using MOBCAL, and a computational estimate for the percentage increase in CCS was calculated from this model structure relative to the CCS of the crystal structure. This enabled the comparison of the %CCS experimental data with the computational estimate for the model containing the crystal structure for GroEL minus one of its subunits and one fully extended GroEL monomer docked to this structure, as reported previously [34].

3. Results and discussion

The effects of acceleration voltage on the spectra and on the excess mass carried by GroEL ions and measured in the spectra are shown in Fig. 1. Panel A contains a plot of GroEL spectra at a range of acceleration voltages. In panel B the excess mass (defined relative to the sequence mass of GroEL) measured in these spectra is plotted against the voltage used to accelerate the ions into the collision cell region of a Q-ToF mass spectrometer. In the low voltage region the measured mass is significantly greater than that calculated from the sequence, but initially it decreases in a linear fashion as acceleration voltage is increased. In our GroEL measurement, the sequence mass is never attained, but the minimum measured mass is approximately 250 Da above the sequence mass. Further increase in the voltage does not remove any additional mass beyond this minimum, even when voltages sufficient to dissociate subunits from the intact protein complex are applied to the ions.

The desolvation profile shown in Fig. 1 clearly indicates that while most of the excess mass carried by the protein complex can be removed through activating the assembly in the gas phase, a finite number of adducts remain bound to the assembly. The two regions of Fig. 1 are evidence for a bimodal adduct population bound to the GroEL 14mer. Most adducts (95%) are lost progressively at acceleration voltages below 100 V indicating weaker binding to the protein complex when compared to the small percentage (5%) that are tightly bound to the assembly and do not dissociate at any acceleration voltage in our experiments. It is interesting to note that the minimum extra mass observed for the GroEL 14mer would correspond to approximately one water molecule or sodium or ammonium ion per subunit. These remaining adducts could be binding specifically to the assembly and may be important in preserving the assembly. It is likely that the weakly bound adduct population arises from incomplete evaporation in the nESI event, potentially leaving a "solvation shell" surrounding some parts of the protein complex, as shown schematically in Fig. 1.

We have reported previously on the importance of complete desolvation in acquiring optimised mass spectra for large protein–protein complexes [23,9,35] and discussed the origin of the excess mass observed in MS measurements. Previous data suggest that the excess mass is primarily composed of non-volatile solution components, and that adding a less volatile buffer salt would cause a measurable increase in both the observed mass and MS peak width at a fixed acceleration voltage. To test this hypothesis, tris acetate, a larger, less volatile salt compared with ammonium acetate, was added in various concentrations to the 200 mM ammo-

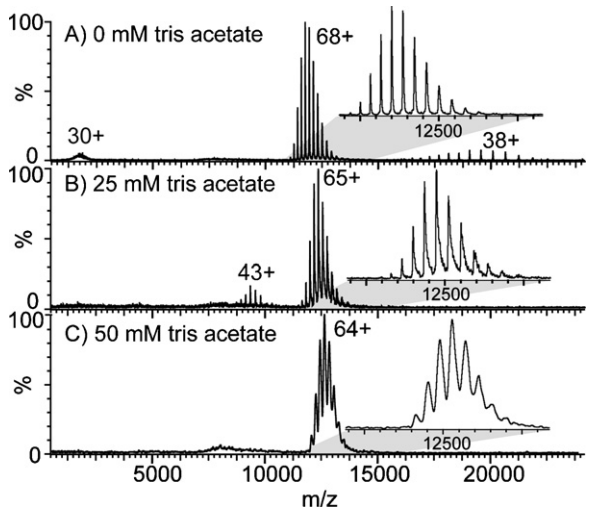

Fig. 2. GroEL mass spectra from solutions containing increasing tris acetate concentrations in 200 mM ammonium acetate acquired at a fixed acceleration voltage of 110 V. The upper spectrum (A) shows data acquired from a solution containing no tris acetate. Dissociation products observed in this spectrum are labelled according to their median charge states (30^+ for monomers and 38^+ for 13mers), whereas the intact 14mer GroEL ion series is the most intense set of peaks around 12000 m/z (68^+). The centre and lower spectra (B and C) are of GroEL in solutions containing 25 and 50 mM tris acetate respectively. The dissociation products observed in the spectrum A are not seen in spectra B and C, and the spectra show decreasing resolution of the charge states as the concentration of tris acetate is increased. The additional ion series seen in spectrum B corresponds to a 7mer of GroEL which is sensitive to the ionic strength of the solution.

nium acetate protein containing solution. Fig. 2 compares the spectra of GroEL in the presence of 0, 25 and 50 mM tris acetate at a collision cell acceleration voltage of 110 V. In the absence of tris acetate, the mass spectra show a well-resolved charge state distribution for the GroEL 14mer centred on the 68^+ ion, and low-intensity dissociation products corresponding to the monomer (at low m/z) and the 13mer (at high m/z) are observed. At the same acceleration voltage the addition of 25 mM tris acetate to the protein containing solution yields broader peaks centred on the 65^+ charge state, and the addition of 50 mM tris acetate results in even broader peaks and a charge envelope centred on 64^+. In the presence of the tris acetate no gas-phase dissociation products are seen at this acceleration voltage.

The data in Fig. 2 indicate that, as expected, the presence of less volatile solution components result in the retention of more buffer molecules/ions. As the collision energy is increased, the ion population in each case can reach a similar level of desolvation, although when tris acetate is present in solution more acceleration voltage is required to achieve the same measured mass and peak width compared to that which can be observed for a buffer solution containing only ammonium acetate (0 mM tris acetate). Deviations in charge state between ion populations created from solutions comprising varying concentrations of tris acetate are difficult to interpret, as it is known that dissociation of monomers (observed in the 0 mM tris acetate case) will influence charge state distributions considerably. On the other hand, the net effect of protein complex dissociation on the charge envelope of protein complex ions is often observed to be a reduction in charge rather than charge enhancement, as higher charge species gain more energy from the applied voltages and dissociate preferentially to those with less charge. This observation then suggests that the mean charge state distributions observed are probably due to the influence of the tris present in the aqueous solution rather than that of charge migration due to collision-induced dissociation (CID). The most pronounced effect observed in this experiment, however, is the increased stability of the protein assemblies upon transfer to the gas phase. This result can be rationalised in part, as tris ions can likely create a larger number of stabilising interactions relative to ammonium ions or water molecules with the protein complex (per ion) due to their larger size. We anticipate that the addition of tris acetate will not alter the bulk properties of the protein containing solution and therefore the droplet size and fission events will remain comparable. In the final stages of desolvation the molecular identity of the adduct population are more likely to impact the structure, as in this regime the loss of each adduct results in the loss of a protein–solution interaction.

The data in Fig. 2 show that, at a fixed acceleration voltage, the greatest mass accuracy and the most extensive dissociation are observed for those ions generated from the solution with the lowest tris acetate concentration. Previous results have indicated that measuring the MS peak width can be used to correct the measured mass of a protein complex for comparison against the sequence mass [23]. The foundation of this method is the observed linear relationship between MS peak width and excess measured mass. In order to further probe the universality of this approach, we measured the relationship between excess measured mass and MS peak width for solutions containing the GroEL 14mer in the presence of 200 mM ammonium acetate and varying amounts of tris acetate (Fig. 3A). Through careful control of instrument parameters, we were able to reproduce the linear relationship between peak width and excess mass across a broad range of acceleration voltages and tris acetate concentrations. This data, therefore, indicate that the linear relationship between mass increase and MS peak width is relatively insensitive to changes in the buffer composition, as all points in Fig. 3A lie within the same prediction interval for the linear relationship determined for the data.

The result shown in Fig. 3A is somewhat surprising, as we originally surmised that the final MS peak width achieved in our experiments is ultimately determined by both the nature of adducts bound to the protein assembly and the dynamics of the desolvation process. However, when compared with our previous results [23] we noted a difference in the gradient determined in Fig. 3A relative to that previously reported. Based on this observation, we probed other variables and instrumental parameters that might alter the linear relationship between peak width and the amount of excess mass measured relative to the sequence mass of GroEL. The experiments performed on different mass spectrometers, including a modified Q-Star XL [44] and a Q-ToF II instrument containing a high pressure sleeve around the hexapole ion guide [45], indicated that the pressure achieved in the first regions of differential pumping can influence the slope of the linear relationship measured between MS peak width and excess mass measured [data not shown]. Based on these results we performed a series of experiments designed to monitor the influence of the pressure in the first region of differential pumping with the observed slope of the relationship shown in Fig. 3B. These results indicate that, over the operating pressure range of the Q-ToF II [37], the slope of the relationship can change by a factor of 4 in a pressure-dependent fashion. This result is interesting, as it indicates that while using higher pressure in the first region of differential pumping can improve MS peak resolution, it does not always provide a concomitant decrease in the excess mass carried by the ions.

A more complete picture of how the addition of less volatile buffer components can influence the excess mass recorded for protein complexes, and by extension the optimum mass accuracy for such assemblies, requires a detailed description of the relationship between acceleration voltage and measured mass for solutions of varying tris acetate concentration (Fig. 4, upper panel). For each experiment, the acceleration voltage is carefully increased (in 10 V increments) in order to capture an accurate description of the desolvation profile of the protein complex ions generated from each solution. The three trends shown in the upper panel of Fig. 4 all exhibit similar profiles, however they differ in the amount of accel-

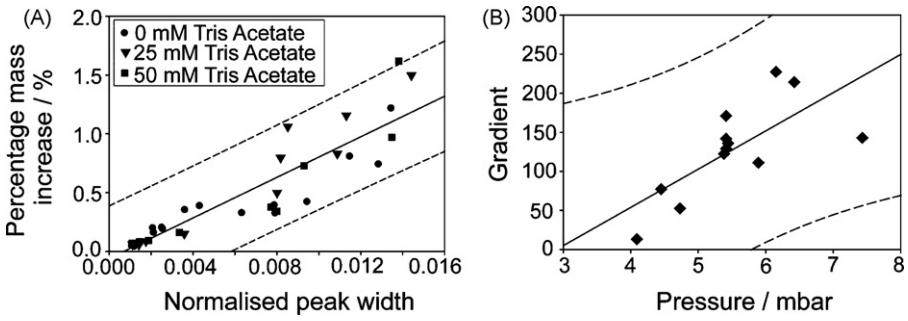

Fig. 3. (A) A plot of percentage mass increase versus normalised peak width for GroEL in solutions containing 0, 25 and 50 mM tris acetate and 200 mM ammonium acetate over a range of activation energies. Black circles: 0 mM tris acetate, black triangles: 25 mM tris acetate, black squares: 50 mM tris acetate, black line: linear fit for the combined data (R^2: 0.85, gradient: 86 ± 5, and intercept: -0.06 ± 0.04), and dashed black lines: 99% prediction interval. (B) A plot of the slope of the relationship derived (as in A) versus the pressure in the first region of differential pumping (R^2: 0.51, gradient: 50 ± 20, and intercept: -140 ± 80), and dashed black lines: 99% prediction interval.

eration voltage required to reach the minimum observed mass of the protein complex. At low acceleration voltages, the mass increase relative to the predicted sequence mass is significantly greater when tris acetate salt is present, although the minimum mass is similar in all experiments. This observation implies that the addition of less volatile tris acetate salt to the buffer does not significantly alter the number of tightly bound adducts, although higher collision energies are needed to achieve the minimum mass of the complex when tris is present in solution. The difference in gradients for the initial desolvation trends in the presence of various concentrations of tris acetate recorded in the upper panel of Fig. 4 allows calculation of a rough estimate for the upper bound collision energy required to remove one tris ion from the complex to be 5 ± 3 meV. This result assumes that tris ions make up the additional loosely bound adduct population which increases as the concentration of tris acetate is raised.

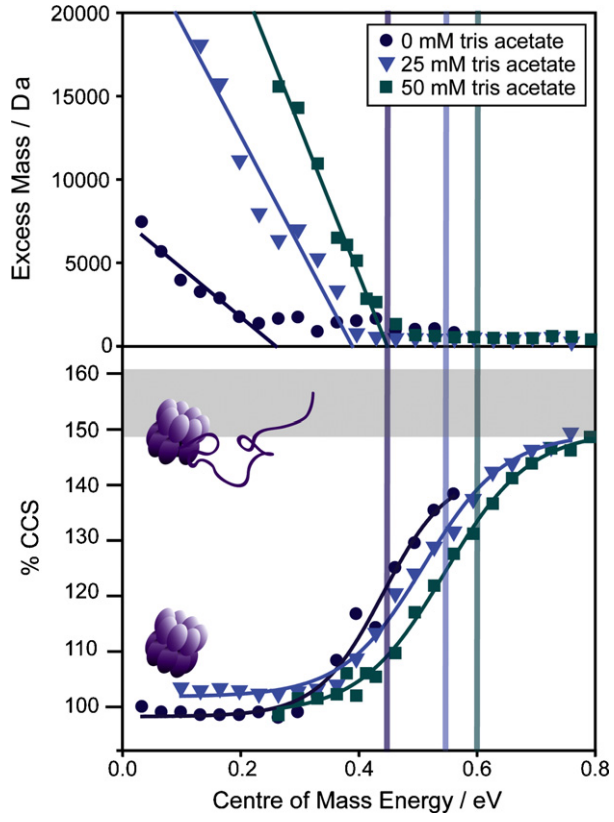

Fig. 4. Plots of observed excess mass (upper panel) and %CCS (lower panel) versus centre-of-mass energy for GroEL 66^+ ions generated from different tris acetate concentrations. Purple circles: 0 mM tris acetate, blue triangles: 25 mM tris acetate, green squares: 50 mM tris acetate. In the lower panel trends are plotted to guide the eye and the vertical lines spanning both panels correspond to the centre-of-mass energies where the intensity of the dissociation products are 50% of the parent intensity. The colour of all lines is coded to match one of the three datasets. The %CCS calculated using the PA and EHSS methods for the fully extended docked monomer is shown as a horizontal grey bar. The schematics shown in the lower panel are illustrations of the structures modelled, the lower image illustrates the GroEL subunit architecture and the upper image shows this same structure with one unfolded subunit. (For interpretation of the references to colour in this figure legend, the reader is referred to the web version of the article.).

The lower panel of Fig. 4 compares the %CCS increase observed for the 66^+ charge state of the GroEL 14mer ions in the same three buffer compositions and energy range monitored in the upper panel of Fig. 4. The data shows a transition in CCS for the GroEL 14mer as a function of centre-of-mass collision energy. At low collision energies, the CCS of the 14mer is constant until a threshold collision energy is reached. At this threshold, the CCS increases until it reaches a maximum value at high collision energy. This same trend is seen for 0, 25 and 50 mM tris acetate concentrations; however, the energy required to reach the threshold collision energy for CCS increase demonstrates a clear dependence upon the tris acetate concentration. Higher collision energies are required to increase the CCS of the ion in higher tris acetate concentrations. While significant amounts of loosely bound buffer molecules still adhere to the protein complex at low collision energies, the CCS of the GroEL 14mer is observed to be constant. An excess of loosely bound buffer molecules does not influence the CCS of large protein complex ions, consistent with our previous results [25]. However, the lack of key bound buffer molecules may influence the CCS by distorting the quaternary structure.

Previously, we have assigned CCS transitions similar to those observed in Fig. 4 to model structures where subunit unfolding within the protein complex has taken place in the gas phase [34]. In those experiments, our analysis revealed that the CCS increase observed for the protein complex did not exceed the computational estimate for a completely extended monomeric unit docked to the rest of the folded structure. This observation is consistent with our results for the GroEL 14mer, where the computational estimate of the %CCS for the 14mer that has a fully extended monomer is indicated by the horizontal band on the lower panel of Fig. 4. According to our measurements, the largest experimental CCS increase achieved by the intact 14mer is approximately 90% of the maximum CCS calculated using this model. This result is consistent with this theory of protein complex dissociation [46,47] and further supports the idea of a long-lived dissociative intermediate state for the protein complex where a single subunit within the assembly has undergone extensive unfolding, rather than models that involve extensive unfolding of many subunits simultaneously.

Additional insight into the structural transitions experienced by the GroEL 14mer as a function of collision energy can be derived by

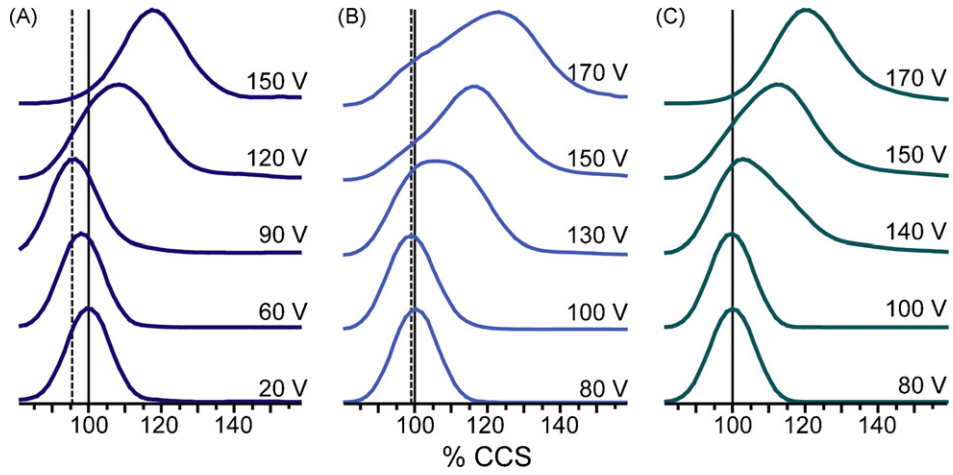

Fig. 5. Drift time plots for the GroEL 62^+ ions in the presence of 0 (purple), 25 (blue) and 50 mM (green) tris acetate in columns A, B, and C respectively. Acceleration voltages are on the right hand side of each plot, ranging from 20 to 170 V. The solid black vertical line marks the centroid of the drift time distribution at the lowest energy. In the absence of tris acetate, GroEL compacts in size (shown by the vertical dashed line), whereas no significant size decrease is observed in the presence of tris acetate. (For interpretation of the references to colour in this figure legend, the reader is referred to the web version of the article.).

comparing the MS data in the upper panel of Fig. 4 with the IM data recorded in the lower panel. Spanning the two panels of Fig. 4 are lines indicating the collision energy at which the ion intensity for dissociation products is 50% of the total ion intensity for each of the three buffer compositions. Increasing tris acetate concentration results in the appearance of dissociation products at higher collision energies. The direct comparison between these two panels allows us to examine the connectivity between the CID process observed by using MS and the protein unfolding process observed by means of IM. Our data confirm that the CID process is indeed linked to the protein unfolding observed by means of IM, since the shift to higher collision energies for the various dissociative transitions observed in MS are mirrored in the IM data. Furthermore, rather than a occupying a well-defined intermediate state, the positioning of the 50% dissociation energy on the IM data indicates that many protein complexes occupying a range of CCS values give rise to the observed dissociation products. Overall, these observations are consistent with the data shown in Fig. 2, and imply that non-specifically bound tris ions can measurably stabilise the GroEL 14mer in the gas phase. It is likely that this stabilisation occurs through the generation of additional stabilising interactions as the larger tris ion has many opportunities for hydrogen bonding.

A detailed investigation of the drift time distributions recorded for the GroEL 14mer reveals evidence of further gas-phase structural transitions. As observed previously for other gas-phase protein–protein complexes [25], the lowest charge states of GroEL have larger CCS values than higher charge states under conditions where the ions are subjected to relatively low collision energies (data not shown). In the case of 62^+ GroEL ions, plots of the drift time distributions as a function of collision energy (Fig. 5) clearly show that the centroid of the distribution recorded decreases prior to a more dramatic increase at higher collision energies (far left panel). In addition, IM data for solutions containing 0, 25, and 50 mM tris acetate are also shown in Fig. 5. On the addition of tris acetate the centroid drift time distribution recorded at low collision energy is constant, as indicated by the position of the vertical bar shown. For both solutions containing tris acetate, no detectable decrease in the centroid of the drift time distribution is observed as the collision energy is increased. For higher charge states of the GroEL 14mer, this decrease in centroid drift time is also not observed. The data in Fig. 5 are consistent with a compaction of the GroEL CCS by about 4% in the absence of tris acetate. Significantly, the addition of tris acetate to the assembly in solution seems to stabilise the complex relative to this structural transition in the gas phase. The observed decrease in CCS for the 14mer cannot be rationalised in terms of the loss of a "solvation shell" around the ion because data in Figs. 2 and 4 indicate a much larger gradient for the weakly bound excess material when tris acetate is added. The decrease in CCS is not observed when tris acetate is added in solution, and we rationalise this decrease in ion size as a reorganisation of the quaternary structure of the molecule. This is consistent with previous results, where we interpreted a similar decrease in CCS to a collapse in the quaternary structure of a ring-like complex [25]. The loss of the central cavity of GroEL could result in a significant reduction in CCS and is the most likely configuration of the smaller GroEL 14mers observed in Fig. 5.

Combining all the data acquired in this work, a general picture can be assembled for the final desolvation stages of GroEL in the absence of lower volatility solution components (Fig. 6, upper panel). The centre-of-mass collision energy is given as a scale bar through the centre of the schematic and the positioning of various structural transitions of the GroEL 14mer are positioned on this axis according to the data presented above. At low collision energies, weakly bound adducts and excess mass from solution is lost (Fig. 4) and this is displayed as a decrease in "solvation shell" size leaving tightly bound material (shown as small coloured circles). After all the weakly bound adducts are removed, the ion internal energy derived from collisions is portioned into disrupting the quaternary structure of the assembly (pictured as a collapsed arrangement of GroEL subunits, see Fig. 5). Increasing the collision energy beyond this stage results in monomer unfolding, reported by a dramatic increase in CCS (Fig. 4). In Fig. 6, we illustrate these unfolded states as primarily being composed of a single disrupted monomer docked to a folded 13mer, as discussed above. At even higher collision energies, dissociation of the protein complex occurs.

There are several important differences to this general picture upon the addition of less volatile buffer salts to the protein complex in solution (Fig. 6, lower panel). These are shown on the same energy axis as the upper panel where no additional lower volatility solution components are added to the solution. Although desolvation is found to largely follow the same general pathway in the presence of lower volatility buffer salt (yellow circles), all structural transitions and dissociation steps are shifted to higher collision energies when compared to ions produced from ammonium acetate buffer. This observation constitutes strong evidence for the added stability conferred to the protein assembly in the presence of less volatile buffer salts. Furthermore, the quaternary structure rearrangement step observed for ions generated from

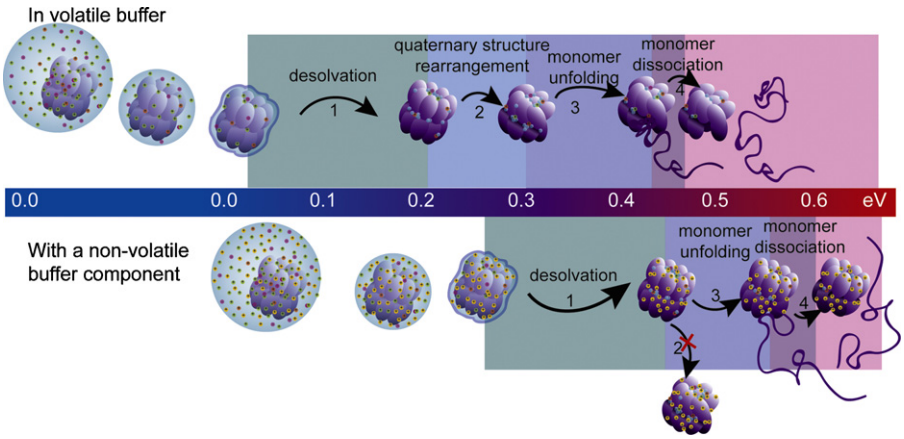

Fig. 6. Schematic of GroEL desolvation with and without tris acetate in the buffer solution. Tris ions, which are less volatile than ammonium ions, are indicated by yellow circles as the non-volatile component. The scale bar in the middle is taken from data acquired on the GroEL 14mer and is representative of the centre-of-mass collision energy at which the various transitions occur. GroEL is represented as a 14mer of purple ellipses arranged in two stacked rings. The initial blue circles, containing various buffer components are indicative of the nESI droplet evaporating to yield protein ions. The upper schematic represents data collected for ions generated from ammonium acetate. The lower schematic depicts the observations for those ions having tris acetate added to the ammonium acetate buffer. We have identified 4 discrete transitions in either composition or structure for gas-phase protein complexes: In stage 1 weakly bound adducts and buffer molecules are removed. During stage 2 the quaternary structure of the complex is reorganised to form a more compact structure than initially adopted. This stage only occurs in the absence of tris counter ions. In stage 3 unfolding of a monomeric unit within the complex occurs and is closely followed by stage 4 where dissociation products are observed. (For interpretation of the references to colour in this figure legend, the reader is referred to the web version of the article.).

solutions containing only ammonium acetate buffer is not observed when tris acetate is added. Taken together, these two observations describe the scope of the stabilisation provided by modifying the composition of ions bound to the protein assembly in the gas phase. Specifically, the evidence in this work shows that the addition of larger, less volatile ions to the protein complex seemingly stabilises all levels of protein structure from large-scale rearrangement in the gas phase.

4. Conclusions

Optimising both MS and IM datasets relies heavily on understanding and manipulating the bound aqueous buffer molecules and ions in the gas phase. Here, we demonstrate that the final stages of desolvation for a large protein complex can be manipulated by simple modifications to the buffer composition prior to subjecting the assembly to nESI MS analysis. IM–MS data show that buffer molecules are lost from the protein complex in a fashion indicating two adduct populations adhering to the protein assembly. We have further validated our method [23] for estimating the amount of bound aqueous buffer for proteins of previously unknown mass. This method has also been refined to show that varying the pressure in the first region of differential pumping can influence the observed relationship between MS peak width and the amount of excess mass retained from solution. While the mechanistic details of this pressure dependence are currently under investigation, it is clear that altering the pressure, and thus the energy and number of collisions experienced by the ions, can influence the early steps of protein complex desolvation.

Protein complexes undergo a series of structural transitions in the gas phase as a function of ion internal energy. For ions of GroEL generated from ammonium acetate buffer, these stages can include a compaction step, followed by an increase in size and eventual dissociation of the protein assembly. Data shown here are consistent with previous experiments [25], suggesting that the compaction step observed for GroEL is indicative of the collapse of the cavity within the barrel-like protein complex. In addition, the ultimate size achieved by the GroEL 14mer does not exceed the size increase predicted by models composed of a completely extended GroEL monomer docked to the remaining folded subunits. This result is also consistent with a dissociation model where subunits are unfolded in a largely sequential fashion rather than in parallel [46,47].

The addition of lower volatility solution components result in gas-phase protein complex ions that are more stable than those generated from solutions that do not contain such components. Notably, protein complexes where the larger, less volatile tris ion has added to or replaced some cations bound to the protein complex are seemingly stabilised against gross rearrangements in quaternary structure. This observation will have a significant impact on our approach to IM–MS experiments in the future. An approach similar to the one described here could be extended to support the vast array of experiments aimed at preserving fragile protein structures in the gas phase for structural analysis [48–50].

Acknowledgements

The authors thank Justin Benesch and Tara Pukala for assistance with sample preparation and Daniel Barsky for molecular modelling assistance. Additionally, Alan Sandercock, Justin Benesch and Matthew Bush are thanked for critical comments. JF is funded by an EPSRC/RSC studentship, CVR is supported by the Royal Society, and BTR is a Waters Research Fellow.

References

[1] E.N. Kitova, M. Seo, P.-N. Roy, J.S. Klassen, Elucidating the intermolecular interactions within a desolvated protein-ligand complex. An experimental and computational study, J. Am. Chem. Soc. 130 (2008) 1214–1226.
[2] J.A. Loo, Electrospray ionization mass spectrometry: a technology for studying noncovalent macromolecular complexes, Int. J. Mass Spectrom. 200 (2000) 175–186.
[3] J.L.P. Benesch, B.T. Ruotolo, D.A. Simmons, C.V. Robinson, Protein complexes in the gas phase: technology for structural genomics and proteomics, Chem. Rev. 107 (2007) 3544–3567.
[4] M. Sharon, C.V. Robinson, The role of mass spectrometry in structure elucidation of dynamic protein complexes, Annu. Rev. Biochem. 76 (2007) 167–193.
[5] E. van Duijn, P.J. Bakkes, R.M.A. Heeren, R.H.H. van den Heuvel, H. van Heerikhuizen, S.M. van der Vies, A.J.R. Heck, Monitoring macromolecular complexes involved in the chaperonin-assisted protein folding cycle by mass spectrometry, Nat. Methods 2 (2005) 371–376.
[6] C.S. Kaddis, S.H. Lomeli, S. Yin, B. Berhane, M.I. Apostol, V.A. Kickhoefer, L.H. Rome, J.A. Loo, Sizing large proteins and protein complexes by electrospray ionization mass spectrometry and ion mobility, J. Am. Soc. Mass Spectrom. 18 (2007) 1206–1216.

[7] M. Sharon, T. Taverner, X.I. Ambroggio, R.J. Deshaies, C.V. Robinson, Structural organization of the 19S proteasome lid: insights from MS of intact complexes, PLoS Biol. 4 (2006) e267.
[8] M. Zhou, A.M. Sandercock, C.S. Fraser, G. Ridlova, E. Stephens, M.R. Schenauer, T. Yokoi-Fong, D. Barsky, J.A. Leary, J.W. Hershey, J.A. Doudna, C.V. Robinson, Mass spectrometry reveals modularity and a complete subunit interaction map of the eukaryotic translation factor eIF3, Proc. Natl. Acad. Sci. USA 105 (2008) 18139–18144.
[9] H. Hernández, C.V. Robinson, Determining the stoichiometry and interactions of macromolecular assemblies from mass spectrometry, Nat. Protoc. 2 (2007) 715–726.
[10] H. Hernández, A. Dziembowski, T. Taverner, B. Seraphin, C.V. Robinson, Subunit architecture of multimeric complexes isolated directly from cells, EMBO Rep. 7 (2006) 605–610.
[11] H. Videler, L.L. Ilag, A.R. McKay, C.L. Hanson, C.V. Robinson, Mass spectrometry of intact ribosomes, FEBS Lett. 579 (2005) 943–947.
[12] C. Uetrecht, C. Versluis, N.R. Watts, W.H. Roos, G.J.L. Wuite, P.T. Wingfield, A.C. Steven, A.J.R. Heck, High-resolution mass spectrometry of viral assemblies: molecular composition and stability of dimorphic hepatitis B virus capsids, Proc. Natl. Acad. Sci. USA 105 (2008) 9216–9220.
[13] A.J. Painter, N. Jaya, E. Basha, E. Vierling, C.V. Robinson, J.L.P. Benesch, Real-time monitoring of protein complexes reveals their quaternary organization and dynamics, Chem. Biol. 15 (2008) 246–253.
[14] C.A. Keetch, E.H. Bromley, M.G. McCammon, N. Wang, J. Christodoulou, C.V. Robinson, L55P transthyretin accelerates subunit exchange and leads to rapid formation of hybrid tetramers, J. Biol. Chem. 280 (2005) 41667–41674.
[15] M.S. Wilm, M. Mann, Electrospray and Taylor-cone theory Dole's beam of macromolecules at last? Int. J. Mass Spectrom. 136 (1994) 167–180.
[16] M. Wilm, M. Mann, Analytical properties of the nanoelectrospray ion source, Anal. Chem. 68 (1996) 1–8.
[17] M. Dole, L.L. Mack, R.L. Hines, Molecular Beams of Macroions, J. Chem. Phys. 49 (1968) 2240–2249.
[18] J.F. de la Mora, Electrospray ionization of large multiply charged species proceeds via Dole's charged residue mechanism, Anal. Chim. Acta 406 (2000) 93–104.
[19] I.A. Kaltashov, A. Mohimen, Estimates of protein surface areas in solution by electrospray ionization mass spectrometry, Anal. Chem. 77 (2005) 5370–5379.
[20] J.L.P. Benesch, C.V. Robinson, Mass spectrometry of macromolecular assemblies: preservation and dissociation, Curr. Opin. Struct. Biol. 16 (2006) 245–251.
[21] R.D. Smith, J.A. Loo, C.J. Barinaga, C.G. Edmonds, H.R. Udseth, Collisional activation and collision-activated dissociation of large multiply charged polypeptides and proteins produced by electrospray ionization, J. Am. Soc. Mass Spectrom. 1 (1990) 53–65.
[22] J.P. Speir, M.W. Senko, D.P. Little, J.A. Loo, F.W. McLafferty, High-resolution tandem mass spectra of 37–67 kDa proteins, J. Mass Spectrom. 30 (1995) 39–42.
[23] A.R. McKay, B.T. Ruotolo, L.L. Ilag, C.V. Robinson, Mass measurements of increased accuracy resolve heterogeneous populations of intact ribosomes, J. Am. Chem. Soc. 128 (2006) 11433–11442.
[24] L.P. Tolic, J.E. Bruce, Q.P. Lei, G.A. Anderson, R.D. Smith, In-trap cleanup of proteins from electrospray ionization using soft sustained off-resonance irradiation with Fourier transform ion cyclotron resonance mass spectrometry, Anal. Chem. 70 (1998) 405–408.
[25] B.T. Ruotolo, K. Giles, I. Campuzano, A.M. Sandercock, R.H. Bateman, C.V. Robinson, Evidence for macromolecular protein rings in the absence of bulk water, Science 310 (2005) 1658–1661.
[26] A. Baumketner, S.L. Bernstein, T. Wyttenbach, G. Bitan, D.B. Teplow, M.T. Bowers, J.-E. Shea, Amyloid beta-protein monomer structure: a computational and experimental study, Protein Sci. 15 (2006) 420–428.
[27] B.T. Ruotolo, C.V. Robinson, Aspects of native proteins are retained in vacuum, Curr. Opin. Struct. Biol. 10 (2006) 402–408.
[28] M.F. Jarrold, D.E. Clemmer, Ion mobility measurements and their applications to clusters and biomolecules, J. Mass Spectrom. 32 (1997) 577–592.
[29] B.C. Bohrer, S.I. Merenbloom, S.L. Koeniger, A.E. Hilderbrand, D.E. Clemmer, Biomolecule analysis by ion mobility spectrometry, Annu. Rev. Anal. Chem. 1 (2008) 293–327.
[30] T. Wyttenbach, M.T. Bowers, Intermolecular interactions in biomolecular systems examined by mass spectrometry, Annu. Rev. Phys. Chem. 58 (2007) 511–533.
[31] C.S. Hoaglund-Hyzer, A.E. Counterman, D.E. Clemmer, Anhydrous protein ions, Chem. Rev. 99 (1999) 3037–3080.
[32] M.F. Jarrold, Unfolding, refolding, and hydration of proteins in the gas phase, Acc. Chem. Res. 32 (1999) 360–367.
[33] B.T. Ruotolo, J.L.P. Benesch, A.M. Sandercock, S.-J. Hyung, C.V. Robinson, Ion mobility-mass spectrometry analysis of large protein complexes, Nat. Protoc. 3 (2008) 1139–1152.
[34] B.T. Ruotolo, S.-J. Hyung, P.M. Robinson, K. Giles, R.H. Bateman, C.V. Robinson, Ion mobility–mass spectrometry reveals long-lived, unfolded intermediates in the dissociation of protein complexes, Angew. Chem. Int. Ed. 46 (2007) 8001–8004.
[35] F. Sobott, C.V. Robinson, Characterising electrosprayed biomolecules using tandem-MS—the noncovalent GroEL chaperonin assembly, Int. J. Mass Spectrom. 236 (2004) 25–32.
[36] K. Braig, Z. Otwinowski, R. Hegde, D.C. Boisvert, A. Joachimiak, A.L. Horwich, P.B. Sigler, The crystal structure of the bacterial chaperonin GroEL at 2.8 Å, Nature 371 (1994) 578–586.
[37] F. Sobott, H. Hernández, M.G. McCammon, M.A. Tito, C.V. Robinson, A tandem mass spectrometer for improved transmission and analysis of large macromolecular assemblies, Anal. Chem. 74 (2002) 1402–1407.
[38] S.D. Pringle, K. Giles, J.L. Wildgoose, J.P. Williams, S.E. Slade, K. Thalassinos, R.H. Bateman, M.T. Bowers, J.H. Scrivens, An investigation of the mobility separation of some peptide and protein ions using a new hybrid quadrupole/travelling wave IMS/oa-ToF instrument, Int. J. Mass Spectrom. 261 (2007) 1–12.
[39] A.K. Shukla, J.H. Futrell, Collisional activation and dissociation of polyatomic ions, Mass Spectrom. Rev. 12 (1993) 211–255.
[40] M.F. Mesleh, J.M. Hunter, A.A. Shvartsburg, G.C. Schatz, M.F. Jarrold, Structural information from ion mobility measurements: effects of the long-range potential, J. Phys. Chem. 100 (1996) 16082–16086.
[41] A.A. Shvartsburg, M.F. Jarrold, An exact hard-spheres scattering model for the mobilities of polyatomic ions, Chem. Phys. Lett. 261 (1996) 86–91.
[42] K. Giles, J.L. Wildgoose, D. Langridge, Determining ion mobility values using a travelling wave separator, in: 56th Meeting of the American Society for Mass Spectrometry, Denver, CO, USA, 2008.
[43] D. Ritchie, High-order analytic translation matrix elements for real-space six-dimensional polar Fourier correlations, J. Appl. Crystallogr. 38 (2005) 808–818.
[44] I.V. Chernushevich, B.A. Thomson, Collisional cooling of large ions in electrospray mass spectrometry, Anal. Chem. 76 (2004) 1754–1760.
[45] R.H.H. van den Heuvel, E. van Duijn, H. Mazon, S.A. Synowsky, K. Lorenzen, C. Versluis, S.J.J. Brouns, D. Langridge, J. vanderOost, J. Hoyes, A.J.R. Heck, Improving the performance of a quadrupole time-of-flight instrument for macromolecular mass spectrometry, Anal. Chem. 78 (2006) 7473–7483.
[46] I. Sinelnikov, E.N. Kitova, J.S. Klassen, Influence of coulombic repulsion on the dissociation pathways and energetics of multiprotein complexes in the gas phase, J. Am. Soc. Mass Spectrom. 18 (2007) 617–631.
[47] J.L.P. Benesch, J.A. Aquilina, B.T. Ruotolo, F. Sobott, C.V. Robinson, Tandem mass spectrometry reveals the quaternary organization of macromolecular assemblies, Chem. Biol. 13 (2006) 597–605.
[48] J. Oomens, N. Polfer, D.T. Moore, L.v.d. Meer, A.G. Marshall, J.R. Eyler, G. Meijer, G.v. Helden, Charge-state resolved mid-infrared spectroscopy of a gas-phase protein, Phys. Chem. Chem. Phys. 7 (2005) 1345–1348.
[49] H.N. Chapman, A. Barty, M.J. Bogan, S. Boutet, M. Frank, S.P. Hau-Riege, S. Marchesini, B.W. Woods, S. Bajt, W.H. Benner, R.A. London, E. Plonjes, M. Kuhlmann, R. Treusch, S. Dusterer, T. Tschentscher, J.R. Schneider, E. Spiller, T. Moller, C. Bostedt, M. Hoener, D.A. Shapiro, K.O. Hodgson, D. van der Spoel, F. Burmeister, M. Bergh, C. Caleman, G. Huldt, M.M. Seibert, F.R.N.C. Maia, R.W. Lee, A. Szoke, N. Timneanu, J. Hajdu, Femtosecond diffractive imaging with a soft-X-ray free-electron laser, Nat. Phys. 2 (2006) 839–843.
[50] N.P. Barrera, N. Di Bartolo, P.J. Booth, C.V. Robinson, Micelles protect membrane complexes from solution to vacuum, Science 321 (2008) 243–246.